Available online at www.sciencedirect.com
ScienceDirect
International Journal of Multiphase Flow 33 (2007) 707–725
International Journal of Multiphase Flow
www.elsevier.com/locate/ijmulflow

On the interaction between two fixed spherical particles

L. Prahl [a,*], A. Hölzer [b], D. Arlov [a], J. Revstedt [a], M. Sommerfeld [b], L. Fuchs [a]

[a] Div. Fluid Mechanics, Lund University, SE-221 00 Lund, Sweden
[b] Inst. Process Engineering, Martin-Luther University, D-06099 Halle (Saale), Germany

Received 20 February 2006; received in revised form 1 February 2007

Abstract

The variation of the drag (C_D) and lift coefficients (C_L) of two fixed solid spherical particles placed at different positions relative each other is studied. Simulations are carried out for particle Reynolds numbers of 50, 100 and 200 and the particle position is defined by the angle between the line connecting the centers of the particles and the free-stream direction (α) and the separation distance (d_0) between the particles. The flow around the particles is simulated using two different methods; the Lattice Boltzmann Method (LBM), using two different computational codes, and a conventional finite difference approach, where the Volume of Solid Method (VOS) is used to represent the particles. Comparisons with available numerical and experimental data show that both methods can be used to accurately resolve the flow field around particles and calculate the forces the particles are subjected to. Independent of the Reynolds number, the largest change in drag, as compared to the single particle case, occurs for particles placed in tandem formation. Compared to a single particle, the drag reduction for the secondary particle in tandem arrangement is as high as 60%, 70% and 80% for $Re = 50$, 100 and 200, respectively. The development of the recirculation zone is found to have a significant influence on the drag force. Depending on the flow situation in-between the particles for various particle arrangements, attraction and repulsion forces are detected due to low and high pressure regions, respectively. The results show that the inter-particle forces are not negligible even under very dilute conditions.
© 2007 Elsevier Ltd. All rights reserved.

Keywords: Dual particles; Interaction; Volume of Solid (VOS); Lattice Boltzmann method (LBM)

1. Introduction

Multiphase flow systems are used for a wide range of industrial applications, and in order to improve the efficiency of these applications it is important to obtain a better understanding of particle dynamics. Generally, industrial applications operate within the particle Reynolds number range 20–300, motivating studies of particle interaction within this interval. Although the stability of the flow past solid spherical particles and the wake formation behind particles previously have been thoroughly investigated, the focus has primarily been on flow around single particles. Thus, there is a lack of knowledge concerning particle interaction

* Corresponding author. Tel.: +46 46 222 4861; fax: +46 46 222 4717.
E-mail address: Lisa.Prahl@vok.lth.se (L. Prahl).

0301-9322/$ - see front matter © 2007 Elsevier Ltd. All rights reserved.
doi:10.1016/j.ijmultiphaseflow.2007.02.001

motivating further research to improve the understanding and developing more advanced models for particle laden flows. Parameters affecting the drag and lift force a particle is subjected to are the number of surrounding particles, the distance and relative position to other particles in the flow, the Reynolds number and the presence of walls. Examining these parameters and their effect on the flow characteristics, may yield a better understanding of the interaction between particles. The data can in turn be used to improve multiphase flow models.

The flow around single spherical particles and the different transition modes the flow undergoes as the Reynolds number is increased have been investigated in numerous studies, for example Fornberg (1988), Johnson and Patel (1999), Kim and Pearlstein (1990) and Lee (2000). For particles placed in an uniform flow at low Reynolds numbers, the flow past single particles are know to be attached and steady. Taneda (1956) observed that as the Reynolds number reaches a value of approximately 24, a steady axisymmetric recirculation zone is formed as the boundary layer is separating from the particle. More recent studies have reported this first transition to occur at $Re = 20$ (Johnson and Patel, 1999). With increasing Reynolds number the wake downstream a particle increases and the axisymmetry in the wake structure is lost as the Reynolds number reaches a value of 210–212 (Johnson and Patel, 1999; Natarajan and Acrivos, 1993; Taneda, 1956; Tomboulides and Orszag, 2000). However, the flow stays stable until the third transition mode occurs, where the recirculation zone looses its stability and the flow becomes unsteady. The third transition has been reported by Natarajan and Acrivos (1993) to occur at a Re of 277.5, whereas Tomboulides and Orszag (2000) observed the third mode to occur in the interval $Re = 270$–285 and Johnson and Patel (1999) predicted a value within the range $Re = 270$–280. Although the motion is now unsteady, the flow still exhibits time periodicity and planar symmetry around the plane where the shedding process is initiated.

Considering the flow past a single particle, the question of what effect the introduction of a second particle will have on the flow field arises. Regarding flow past dual particles at low Reynolds numbers, the most general studies are the theoretical works presented by Smoluchowski (1911) and Happel and Brenner (1965) who calculated the drag, lift and torque of two spheres moving with the same velocity in a still fluid using the method of reflections. For the case of two spheres placed in line, Faxen (1925) extended Smoluchowskis solution for the drag to higher order. Stimson and Jeffery (1926), with a corrigendum by Faxen (1927), solved the same problem using polar coordinates finding an exact solution for the drag force for two particles with equal diameter and velocity. For two spheres placed in line and separation distances larger than four particle diameters, the solutions of Smoluchowski (1911), Happel and Brenner (1965), Faxen (1927) and Stimson and Jeffery (1926) agree almost completely. Among the first experimental studies that considers the interaction between particles, still at low Reynolds numbers, are the works by Eveson et al. (1959), Happel and Pfeffer (1960) and Rowe and Henwood (1961). Happel and Pfeffer (1960) observed an increase in terminal velocity for two particles falling in tandem formation in a viscous fluid compared to an isolated particle, this is in turn equivalent to a reduced drag. In more recent work, both experimentally and numerically, flow past particles in a larger range of Reynolds numbers have been investigated. Kim et al. (1993) investigated numerically the dependency of drag, lift and momentum coefficients on particle separation distance for particles held fixed in a side-by-side arrangement, i.e. the centers of the particles are connected to a line perpendicular to the flow direction. The same particle formation was numerically and experimentally investigated by Folkersma et al. (2000) and Brydon and Thompson (2001) by varying the separation distance between the particles. Particles placed side-by-side and in tandem formations are the two most frequently investigated dual particle arrangement. Both particle formations mentioned above were investigated experimentally by Chen and Lu (1999) and numerically by Tsuji et al. (2003). These studies examined the dependency of wake structure, flow separation and drag effects on inter-particle distance and Reynolds number. Chen and Lu (1999) also considered three particles arranged side-by-side. Further, Liang et al. (1996) investigated five different dual particle arrangements changing the particle position in relation to the flow direction. An extended study of particle interaction was presented by Olsson and Fuchs (1998) and Chen and Wu (2000), where all positions as one particle is moved around a reference particle were considered. A common conclusion in the aforementioned studies is that the separation distance plays an important role on the drag of interacting particles.

In general, increasing the Reynolds number decreases the drag force. When two particles are held fixed in a side-by-side formation at intermediate and high Reynolds numbers, the drag force increases as the separation distance between the particles decreases. Furthermore, at small distances and relatively small Reynolds

numbers (~100), with the particles almost in contact, the flow is reported to consider the particles as a single body due to a blockage effect (Folkersma et al., 2000; Olsson and Fuchs, 1998; Tsuji et al., 2003). This blockage effect, caused by the high-pressure region between the particles, forces the fluid to move away from the gap and move around the particles, inducing repulsion. Kim et al. (1993) and Folkersma et al. (2000) found that the particles repelled each other at small separation distances and weakly attracted each other at intermediate separation distances. However, as the Reynolds number is increased, a "nozzle effect", i.e. high velocity in the gap between the particles was observed by Tsuji et al. (2003). The "nozzle effect" results in a shift of front stagnation points of the two particles which in turn causes repulsion.

For particles in a tandem arrangement, the high-pressure region in front of the downstream particle is interferring with the low pressure region behind the upstream particle. Because of these pressure interferences and a "slipstream effect", i.e. the trailing particle experiences a smaller flow velocity, the leading particle will be subjected to a larger drag force than the trailing particle, although it is smaller than compared to the drag of a single particle. As the particles are moved further apart, the drag force gradually levels of to the value of an isolated particle. The parameter strongly influencing the drag force for this type of arrangement appears to be whether the trailing particle is in the wake of the upstream particle or not (Olsson and Fuchs, 1998; Zhu et al., 1994). Particles positioned in tandem are not subjected to any lift force for Reynolds number less than 210. The lift force increases with decreasing distance between the particles.

The main purpose of this paper is to study in detail the particle–particle interaction at intermediate Reynolds numbers, focusing on the variation of the drag and lift coefficients as compared to the single particle case. The distance and angle used to define the particle position, together with the particle Reynolds number are taken as free parameters. Also, the performance of two conceptually independent numerical approaches are compared.

2. Numerical methods

Two different numerical approaches used for the computations; first a conventional incompressible Navier–Stokes solver combined with the Volume of Solid (VOS) Method to represent the particle phase and secondly, the Lattice Boltzmann Method (LBM), based on the Boltzmann equation.

2.1. Volume of Solid Method

The Volume of Solid (VOS) Method (Lörstad and Fuchs, 2001), based on the Volume of Fluid (VOF) approach, is used to represent the spherical particles. However, in VOS, the "second fluid" is a solid body assumed to have an infinite viscosity. Since the shear stresses are nearly constant due to the fact that viscous forces are dominating close to the surface, combined with the assumed infinite viscosity of the solid phase, the averaged viscosity can be represented by the following equation:

$$\mu = \frac{\mu_l}{\alpha} \tag{1}$$

where α is the phase variable representing the amount of fluid in each cell, $0 < \alpha < 1$, and μ_l is the dynamic viscosity of the continuous (liquid) phase. Cells containing the solid phase ($\alpha = 0$) will be blocked since there is no flow inside the solid body, and no computations will be carried out for these cells. With a constant density, (1) can be written as

$$\nu = \frac{\nu_l}{\alpha} \tag{2}$$

with ν_l representing the kinematic viscosity of the continuous (liquid) phase. Using the relation above, the viscosity ratio term, $\delta\nu$, can be defined as

$$\delta\nu = \frac{\nu_l}{\nu_l} = \frac{1}{\alpha} \tag{3}$$

It should be noted that in most computational cells, the viscosity average will have the value of unity. With the definition of the viscosity term, as stated in (3), the continuity and momentum equations governing an isothermal, incompressible flow of a Newtonian fluid are as follows:

$$\frac{\partial u_i}{\partial x_i} = 0 \tag{4}$$

$$\frac{\partial u_i}{\partial t} + u_j \frac{\partial u_i}{\partial x_j} = -\frac{\partial p}{\partial x_i} + \frac{1}{Re}\frac{\partial}{\partial x_j}\left(\delta v \frac{\partial u_i}{\partial x_j} + \frac{\partial u_j}{\partial x_i}\right) \tag{5}$$

with p and Re representing the pressure and the Reynolds number ($Re = \rho UL/\mu$), respectively. Eqs. (4) and (5) are discretized on a Cartesian staggered grid using second-order central differences for all spatial derivatives except for the convective terms where a first-order upwind scheme is used. To improve the accuracy without loosing any numerical stability, a defect correction method (Gullbrand et al., 2001) is used to obtain third-order accuracy for convective terms and fourth-order for the remaining terms. A multi-grid method is applied within each time step in order to increase the computational efficiency.

Integrating the steady Navier–Stokes equations over a control volume and transforming this volume integral into a surface integral by using Gauss theorem, the following equation is obtained:

$$F_{\mathrm{h}} = \int\int_{\Gamma} \left(u_i u_j n_j + p n_i \delta_{ij} - \frac{1}{Re}\left(\frac{\partial u_i}{\partial x_j} + \frac{\partial u_j}{\partial x_i}\right) n_j \right) \mathrm{d}\Gamma \tag{6}$$

where Γ is the surface of a control volume, n_i is the unit vector normal to the surface and δ_{ij} is Dirac's distribution function. Here the control volume is created by subtracting the particle from a surrounding cubical box. By integrating equation (6) on the outer surfaces of this control volume, i.e. the faces of the cubic, the forces acting on an object are obtained.

2.2. Lattice Boltzmann Method

The second method used in the present study is the Lattice Boltzmann Method (LBM), an alternative approach to conventional continuum methods. Instead of being based on conservation laws formulated at continuum level, LBM solves the Boltzmann equation (7) describing the fluid flow on a molecular level:

$$\frac{\partial f}{\partial t} + \bar{v} \cdot \nabla f = \left(\frac{\partial f}{\partial t}\right)_{\text{collision}} \tag{7}$$

The probability of finding a number of molecules with a certain velocity, $\bar{v}$, at a certain position, $\bar{x}$, and time, t, is represented by the real distribution function, $f(\bar{x}, \bar{v}, t)$. To describe the process governing the macroscopic transport phenomena, the collision operator, $\left(\frac{\partial f}{\partial t}\right)_{\text{collision}}$, representing the particle distribution for each collision, is used. Velocity and distribution functions are discretized on a finite sets of velocity directions, $\bar{e}_i$.

In order to avoid using the complex collision operator in Eq. (7), the more straightforward BGK collision operator (Bhatnagar et al., 1954), $-\frac{1}{\tau}(f_i - f_i^{\mathrm{eq}})$, is applied. Through the utilization of the BGK operator, the distribution function approaches an equilibrium distribution, f_i^{eq}, known as the Maxwell–Boltzmann distribution, a solution to the Boltzmann equation (7). The rate at which the Maxwell–Boltzmann distribution is reached is determined by the relaxation time, τ. The discretized Boltzmann equation with a BGK operator (Qian et al., 1992), is obtained by discretizing equation (7).

$$f_i(\bar{x} + \bar{e}_i \Delta t, t + \Delta t) - f_i(\bar{x}, t) = -\frac{1}{\tau}(f_i - f_i^{\mathrm{eq}}) \tag{8}$$

Hence, at each time step, Δt, the molecules are transported a distance $\bar{e}_i \Delta t$.

There are different possibilities to discretize the velocity into finite sets of velocity directions, $\bar{e}_i$. In this study, the three-dimensional 19 velocity (D3Q19) model is used, illustrated in Fig. 1 (Qian et al., 1992). The D3Q19 model consists of 6 straight velocity vectors ($i = 1, \ldots, 6$), 12 diagonal velocity vectors

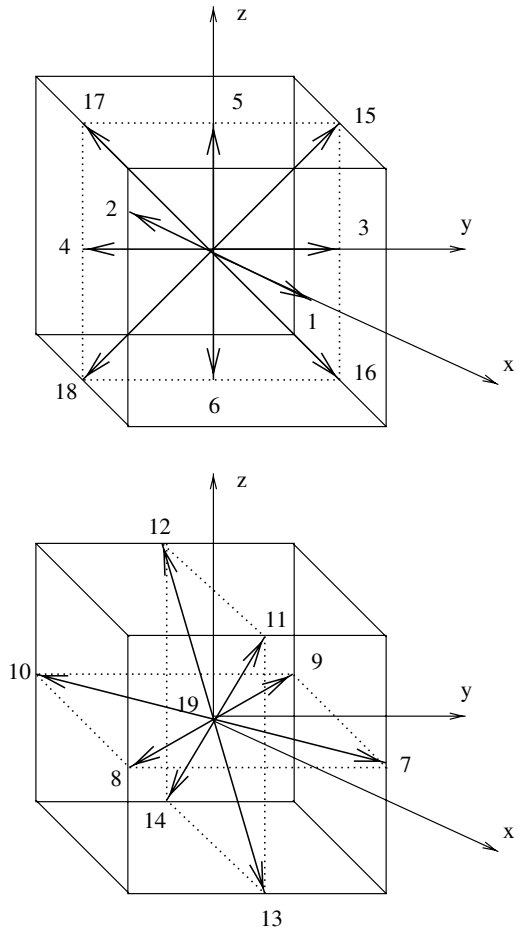

Fig. 1. Discrete velocity vectors of the D3Q19 model.

($i = 7, \ldots, 18$) and one velocity vector for resting molecules, ($i = 19$). Introducing the lattice constant c, defined as $c = \frac{\Delta x}{\Delta t}$, the 19 different velocity directions are

$$\bar{e}_i = \begin{cases} (\pm 1, 0, 0)c, (0, \pm 1, 0)c, (0, 0, \pm 1)c & i = 1, \ldots, 6 \\ (\pm 1, \pm 1, 0)c, (\pm 1, 0, \pm 1)c, (0, \pm 1, \pm 1)c & i = 7, \ldots, 18 \\ (0, 0, 0)c & i = 19 \end{cases}$$

Thus, the equilibrium function, using the D3Q19 model, is defined as follows (Qian et al., 1992):

$$f_i^{\mathrm{eq}}(\bar{x}, t) = w_i \rho \left(1 + 3 \frac{\bar{e}_i \cdot \bar{u}(\bar{x}, t)}{c^2} + \frac{9}{2} \frac{(\bar{e}_i \cdot \bar{u}(\bar{x}, t))^2}{c^4} - \frac{3}{2} \frac{\bar{u}(\bar{x}, t)^2}{c^2} \right) \tag{9}$$

with

$$w_i = \begin{cases} \dfrac{1}{18} & i = 1, \ldots, 6 \\ \dfrac{1}{36} & i = 7, \ldots, 18 \\ \dfrac{1}{3} & i = 19 \end{cases}$$

The kinematic viscosity is determined by the relaxation time through Eq. (10). Density and velocity are obtained locally using Eqs. (11) and (12):

$$v = \frac{1}{6}c^2\Delta t(2\tau - 1) \tag{10}$$

$$\rho(\bar{x}, t) = \sum_{i=0}^{n} f_i(\bar{x}, t) \tag{11}$$

$$\rho(\bar{x}, t)\bar{u}(\bar{x}, t) = \sum_{i=0}^{n} f_i(\bar{x}, t)\bar{e}_i \tag{12}$$

3. Problem set-up

In this study, two equally sized spherical particles with a diameter D are held fixed at several relative positions in a rectangular domain, shown in Fig. 2. The positions are defined by two parameters; the separation distance, d_0, and the angle between the line connecting the centers of the particles and free-stream direction, α, depicted in Fig. 3. The angle is varied from 0° to 360° using 15° increment and the separation distance, d_0, is set to $1.5D$, $3.0D$, $4.5D$ and $6.0D$. Reynolds numbers of 50, 100 and 200 are considered and an uniform velocity profile is applied at the inlet. The remaining boundary conditions are Neumann (for VOS and LBM(II)) and Dirichlet (for LBM(I)) condition at the outlet, symmetry conditions on the lateral boundaries and a no-slip condition on the particle surface. The LBM codes impose a curved no-slip boundary condition with second-order interpolation (Bouzidi et al., 2001) and the force acting on the particle due to the fluid flow is calculated by the momentum exchange between the fluid and the particle on the particle surface (Ladd, 1994). Regarding the velocity components, W is the streamwise velocity whereas U and V represent the transversal velocities. In all result plots, the velocity is scaled by the inlet velocity, $W_{\max}$.

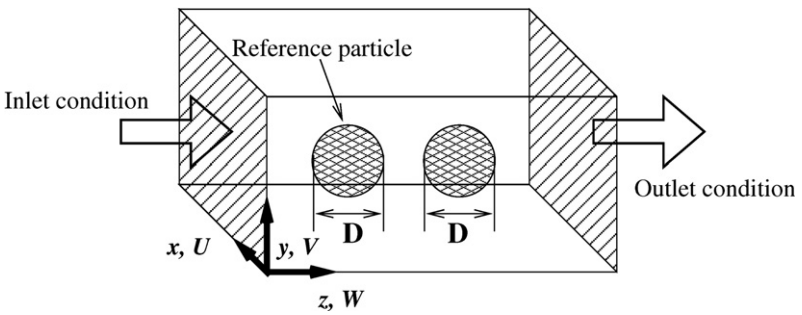

Fig. 2. The computational domain for flow past two particles.

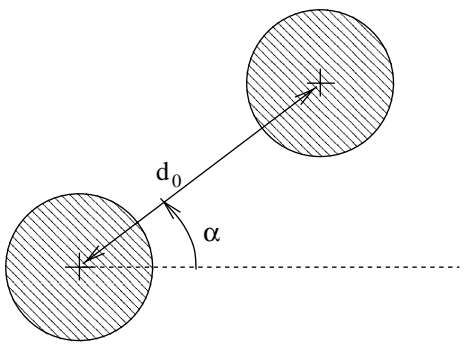

Fig. 3. Definition of separation angle α and distance d_0 for two particles.

Table 1
The geometrical domain, grid resolution and the position of the reference particle

	Domain (x,y,z)	Grid resolution, h	Position reference particle (x,y,z)
VOS	$32D \times 32D \times 32D$	$D/32$	$(16D, 16D, 10D)$
LBM(I)	$9D \times 9D \times 17.5D$	$D/16$	$(4.5D, 4.5D, 6.5D)$
LBM(II)	$6D \times 6D \times 24.5D$	$D/12$	$(3D, 3D, 8D)$

The geometrical domain is set for dual particles when $d_0 = 1.5D$ and $\alpha = 0°$.

The difference between LBM(I) and LBM(II) lies, as mentioned above, in the formulation of the inlet and outlet boundary conditions. Common for both LBM(I) and LBM(II) is that inlet distribution functions, f_i^{inlet}, with desired values of density, ρ^{inlet}, and inflow velocity, u^{inlet}, specifies the inlet velocity profile. However, LBM(I) uses Eq. (13), specified on all inlet boundary nodes for all 19 directions (Dupuis, 2002), whereas LBM(II) applies Eq. (14) only on the boundary nodes in the main flow direction (Aidun et al., 1998). Considering the outlet boundary condition, LBM(I) and LBM(II) use Dirichlet and Neumann (Aidun et al., 1998) boundary condition, respectively, on all outlet boundary nodes:

$$f_i^{\text{inlet}} = \frac{1}{\tau} f_i^{\text{eq}}(\rho^{\text{inlet}}, u^{\text{inlet}}) + \left(1 - \frac{1}{\tau}\right) f_i^{\text{inlet}} \tag{13}$$

$$f_i^{\text{inlet}} = f_i^{\text{inlet}} + 2\rho^{\text{inlet}} w_i u^{\text{inlet}} \tag{14}$$

Considering the dual particle simulations, the domain as well as the grid resolution are adjusted to the performance of the different codes in order to achieve more accurate result, Table 1. For VOS, the geometrical domain is fixed and the particles are positioned inside the pre-defined domain. However, for the two LBM codes the domain size is varied with the position of the downstream particle in order to keep the distance from the particles to the closest lateral boundary constant for all configurations. For LBM(I) the distance between the leading particle and the inlet is $6.5D$, between the trailing particle and the outlet $9.5D$ and between the particles and the closest lateral boundary, the distance is $4.5D$. For LBM(II) the distance between the leading particle and the inlet is $8D$, between the trailing particle and the outlet $15D$ and between the particles and the closest lateral boundary, the distance is $3D$.

In order to ensure correct code implementation and to assess accuracy of the problem set-up an accuracy study and a comparison of VOS and the two versions of LBM are performed for a single particle for different Reynolds number, grid resolution and domain size.

4. Results

4.1. Numerical accuracy and comparison of methods

The three flow solvers used in this study are compared to each other as well as to numerical and experimental data from literature. It should be noted that in all result figures, the drag coefficient is normalized with the drag coefficient of an isolated object for the Reynolds number of interest.

First, a numerical accuracy assessment, varying the domain size and the grid resolution, is performed separately for each solver. Fig. 4, shows the variation of drag with increasing domain size as well as grid resolution for a single particle at a Reynolds number of 100 using VOS. It can be concluded that a grid resolution of $D/h = 64$ only provides a marginal change in drag compared to $D/h = 32$. In terms of grid resolution, the physical length of the boundary layer is within the interval of $\delta/h = 5.12$–9.6 and $\delta/h = 2.56$–4.8 for $Re = 50$ and $Re = 200$, respectively when using $D/h = 32$ (Schlichting, 1955). The same tendency is shown in Fig. 5 where the dependency of grid resolution for (a), the transversal velocity from a section in the recirculation region of the particle and (b), the streamwise velocity in the mid-plane of the domain are displayed. In order to ensure that surrounding boundaries do not influence the flow past a particle, the domain size is set to $32 \times 32 \times 32D$.

Flow around a single particle at a Reynolds number of 50 for different domain sizes and grid resolutions is used in order to investigate the performance of the LBM(I) solver (Fig. 6). According to results shown in

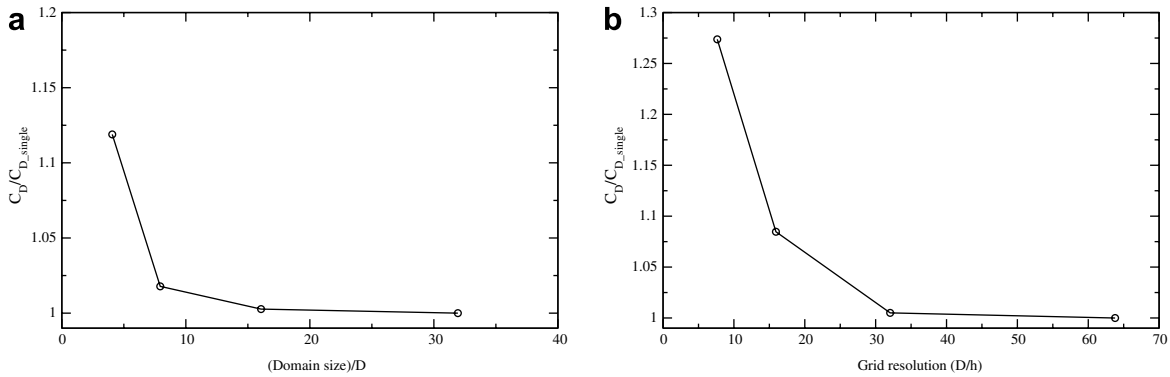

Fig. 4. The normalized C_D varying (a) the domain size in lateral direction and (b) grid resolution using the VOS solver. A single particle at $Re = 100$. A grid resolution of $D/h = 32$ is used in (a) and the domain used in (b) has the dimensions $32 \times 32 \times 32D$.

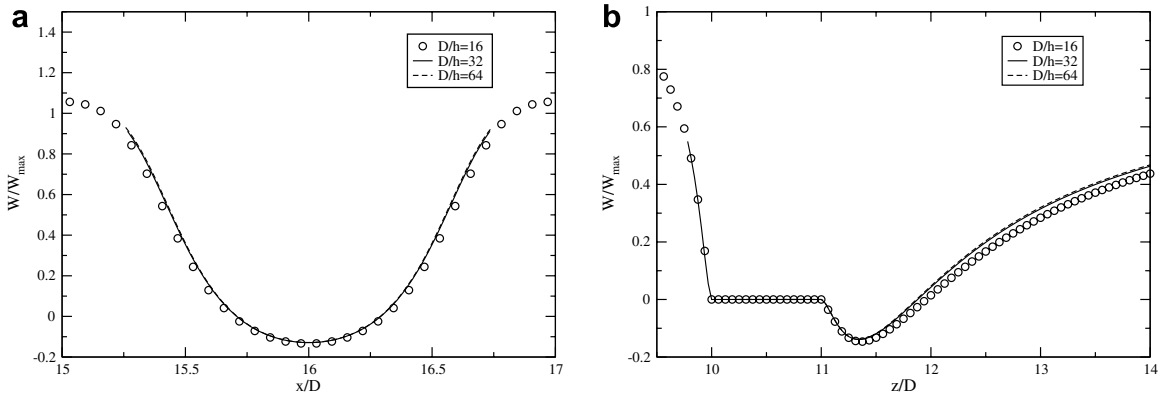

Fig. 5. The velocity profiles for a single particle at $Re = 100$ in flow direction at (a) $(y, z) = (16D, 10.75D)$ and (b) $(x, y) = (16D, 16D)$ using VOS.

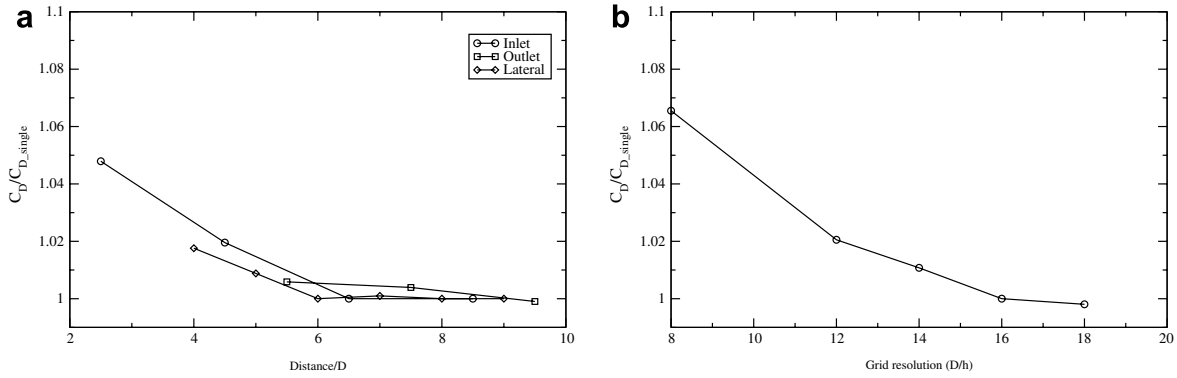

Fig. 6. The normalized C_D when varying (a) the domain size and (b) grid resolution using the LBM(I) solver. A single particle at $Re = 50$. The distance in (a) is the distance from the center of the particle to the inlet, outlet and lateral boundary conditions. A grid resolution of $D/h = 16$ is used in (a) and the domain used in (b) has the dimensions $9 \times 9 \times 16D$.

Fig. 6(b), compared to VOS, LBM(I) appears to be less influenced by the grid resolution. Considering the marginal changes in drag, $D/h = 16$ is chosen for the simulations. The physical length of the boundary layer in terms of grid resolution, is within the interval of $\delta/h = 2.56$–2.4 and $\delta/h = 1.28$–2.4 for $Re = 50$ and

$Re = 200$, respectively for a grid resolution of $D/h = 16$ (Schlichting, 1955). In LBM(I), the domain size is defined by three different directions; the distance from the particle center to inlet boundary as well as the outlet boundary, and the lateral distance between the symmetry boundaries. In order to minimize the influence of the boundaries, the distances to the inlet, outlet and lateral boundaries are set to $6.5D$, $9.5D$ and $4.5D$, respectively, Fig. 6(a). As shown in Fig. 7, the transversal and streamwise velocity profiles show little or no change with increasing grid resolution. Thus, the drag is apparently more affected by the grid resolution than the flow velocity. One explanation for this may be that drag is calculated from the momentum exchange method, where increasing the resolution will increase the number of points representing the particle wall, defined by a curved boundary of second-order interpolation, resulting in a decrease of fluctuation in drag.

The numerical accuracy assessment for the LBM(II) solver is performed for a Reynolds number of 30 for the domain size and the grid resolution, shown in Fig. 8. A grid resolution of $D/h = 12$ is chosen for the simulations. For $D/h = 12$, the physical length of the boundary layer in terms of grid resolution, is within the interval of $\delta/h = 1.92$–3.6 and $\delta/h = 0.96$–1.8 for $Re = 50$ and $Re = 200$ (Schlichting, 1955). A domain size with the particle distances to the inlet, outlet and the lateral boundaries set to $8D$, $15D$ and $3D$, respectively, showed a reduced influence of the boundaries on drag computations. Fig. 9 shows the influence of the velocity profiles as a function of the grid resolution. The wake length is decreasing with increasing grid resolution and for $D/h = 12$ the wake length is $0.16D$.

Secondly, the three different solvers were compared with experimental data from Wieselberger et al. (1923), for flow around a single particle at a Reynolds number of 50. The relative error of the drag coefficient, Table 2,

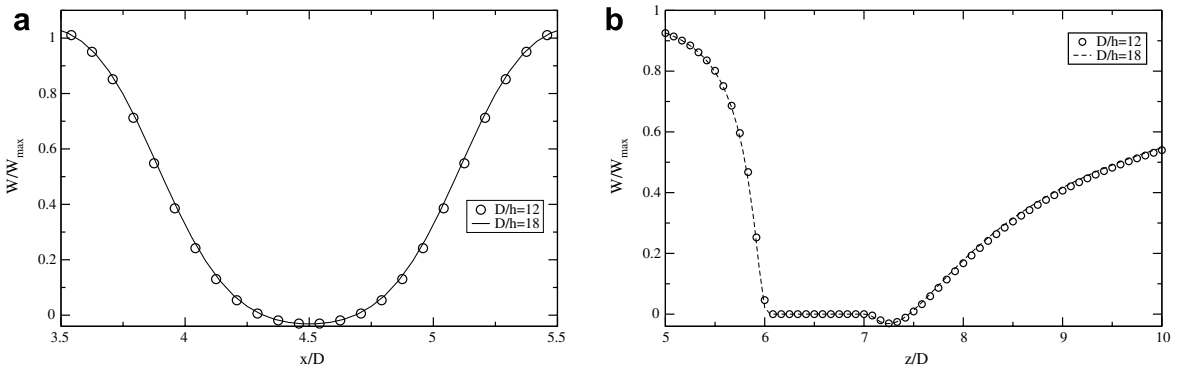

Fig. 7. The velocity profiles for a single particle at $Re = 50$ in flow direction at (a) $(y, z) = (4.5D, 7.25D)$ and (b) $(x, y) = (4.5D, 4.5D)$ using LBM(I).

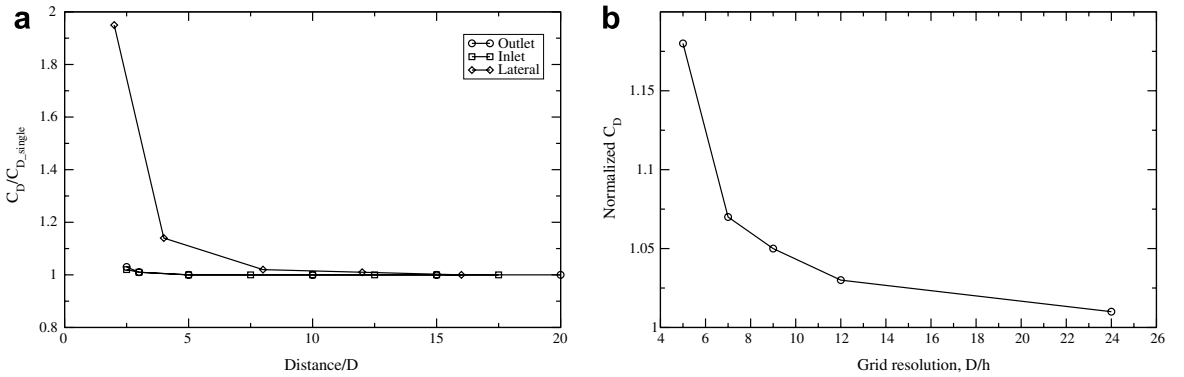

Fig. 8. The normalized CD when varying (a) the domain size and (b) grid resolution using the LBM(II) solver. A single particle at $Re = 30$. The distance in (a) is the distance from the center of the particle to the inlet, outlet and lateral boundary conditions. A grid resolution of $D/h = 4$ is used in (a) and the domain used in (b) has the dimensions $6 \times 6 \times 14D$.

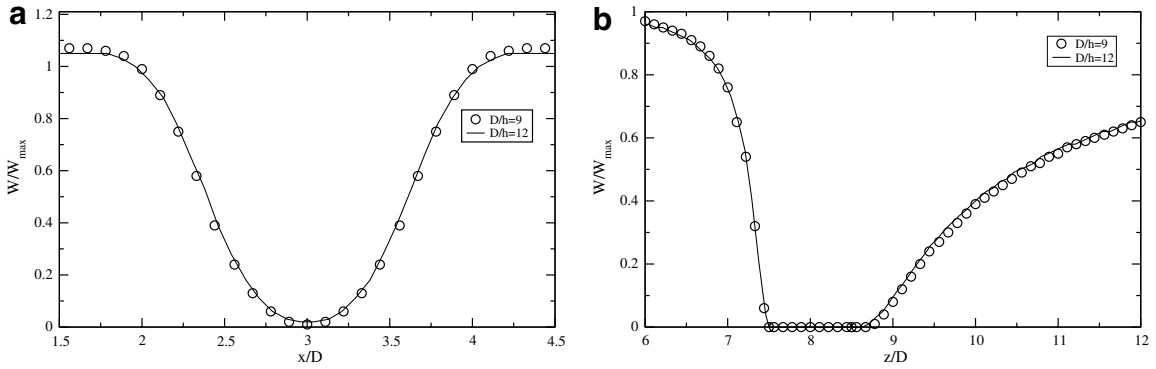

Fig. 9. The velocity profiles for a single particle at $Re = 30$ in flow direction at (a) $(y, z) = (3D, 8.75D)$ and (b) $(x, y) = (3D, 3D)$ using LBM(II).

Table 2
The relative error of drag compared to experiments (Wieselberger et al., 1923) at $Re = 50$

Numerical method	Relative error (%)
VOS	0.6
LBM(I)	2.3
LBM(II)	2.3

using a domain size and grid resolution optimized for each individual solver, shows that results obtained from VOS agree better with experimental data compared to the two LBM solvers. Considering Fig. 10, all three

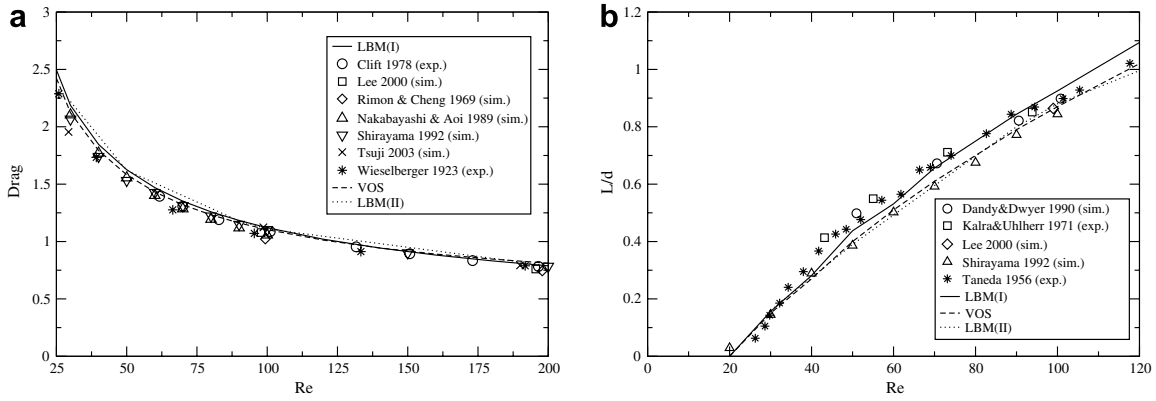

Fig. 10. The (a) drag coefficient and (b) wake length as a function of Reynolds numbers. See the above mentioned references for more details.

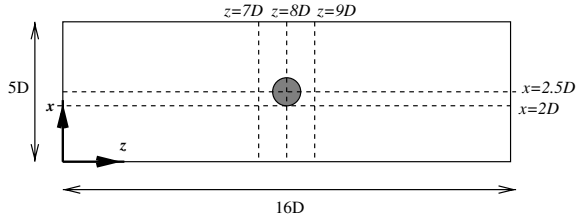

Fig. 11. The geometrical domain for flow past a particle. The dotted lines are the chosen velocity profiles that are to be compared between the different numerical codes. The intersection is taken at $y = 2.5D$.

solvers show good agreement with both numerical and experimental data found in literature for the drag coefficient as well as the wake length for flow around a single particle at a wide range of Reynolds numbers.

Finally, a comparison between the different computational codes is performed by considering the velocity profiles at different sections in the domain for a Reynolds number of 50. The geometrical domain is set to

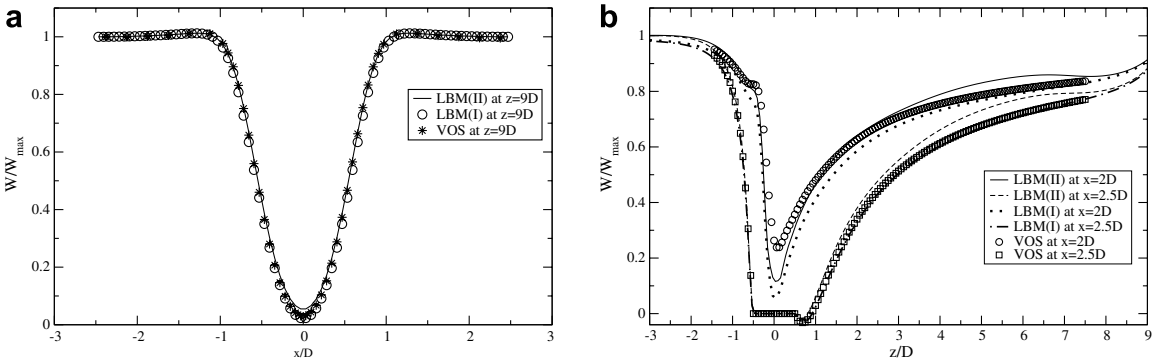

Fig. 12. The velocity profiles in flow direction at (a) $z = 9D$ and (b) $x = 2D, 2.5D$. The intersection is taken at $y = 2.5D$.

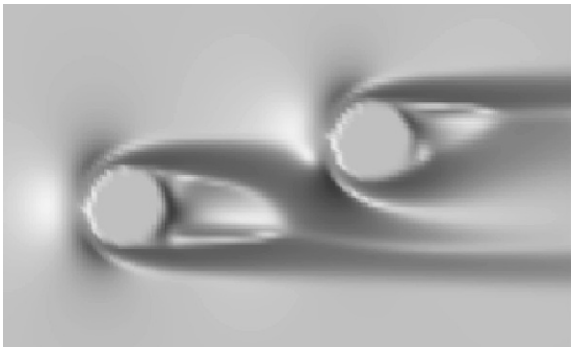

Fig. 13. Contour plot of the streamwise velocity for twin particles at a Reynolds number of 200. $D_0 = 3.0D$ and $\alpha = 15°$.

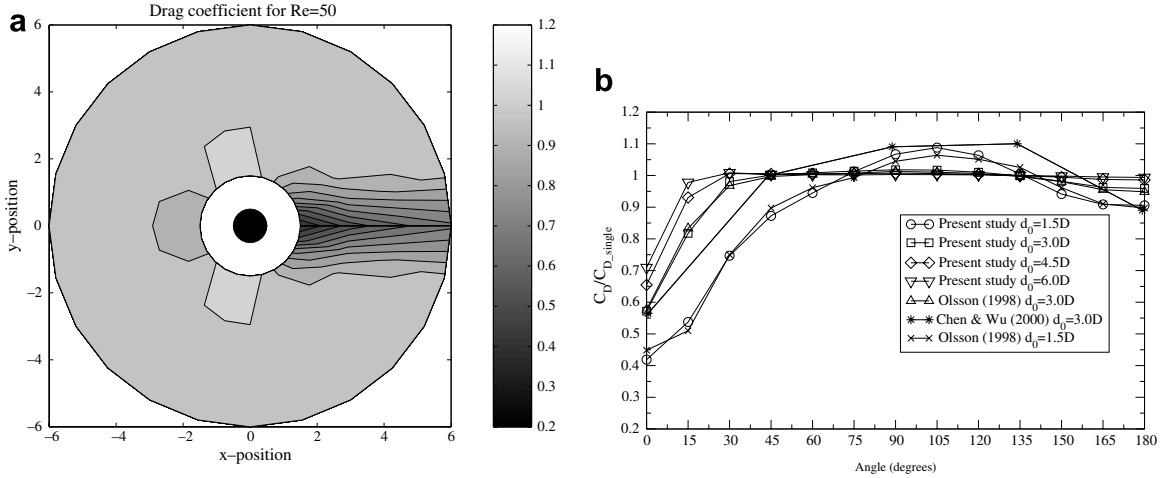

Fig. 14. Normalized drag coefficient at $Re = 50$ with a contour plot (a) and as a function of an angle α (b). The black circle represent the reference particle. Data from VOS computations.

$(x, y, z) = (5D, 5D, 16D)$ with the center of the particle positioned at $(x, y, z) = (2.5D, 2.5D, 8D)$, shown in Fig. 11. A grid resolution of $D/h = 16$ is used for all numerical methods and the results are compared at several sections in the domain. The streamwise velocity profiles at some sections are shown in Fig. 12. Fig. 12(a), depicts the profile of the streamwise velocity component downstream the particle ($z = 9D$). The difference between the solvers is marginal. However, in Fig. 12(b), displaying the streamwise velocity profile at $x = 2D$ and $x = 2.5D$, differences between the solvers are visible. At $x = 2.5D$, LBM(II) predicts a shorter wake length compared to LBM(I) and VOS. According to experimental data, the wake length for a Reynolds number of 50 is $0.43D$ (Taneda, 1956). All three solvers obtained a wake length of $0.39D$. Due to the different outlet boundary conditions, the velocity gradient at the section behind the particle is smaller for LBM(I) compared to LBM(II). Thus, the choice of inlet and outlet conditions has an influence on the results even though the same numerical method is used (LBM). Also, LBM(II) shows an oscillation of velocity with an increase of velocity at $3 < z/D < 7$ and a decrease of velocity further downwards, compared to VOS and LBM(I). For $x = 2D$, the three methods exhibit the same tendency. For this particular case, VOS has a relative error of 7.8% whereas LBM(I) and LBM(II) have relative errors of 3.8% and 5.8%, respectively, compared to Wieselberger et al. (1923). Furthermore, using the same geometrical set-up as in Fig. 11, the computational time has

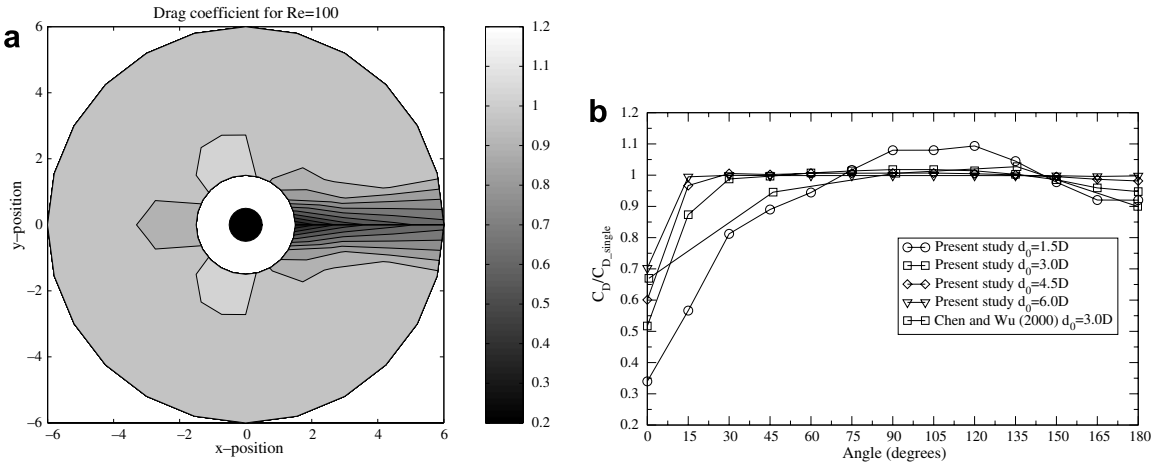

Fig. 15. Normalized drag coefficient at $Re = 100$ with a contour plot (a) and as a function of an angle α (b). The black circle represent the reference particle. Data from VOS computations.

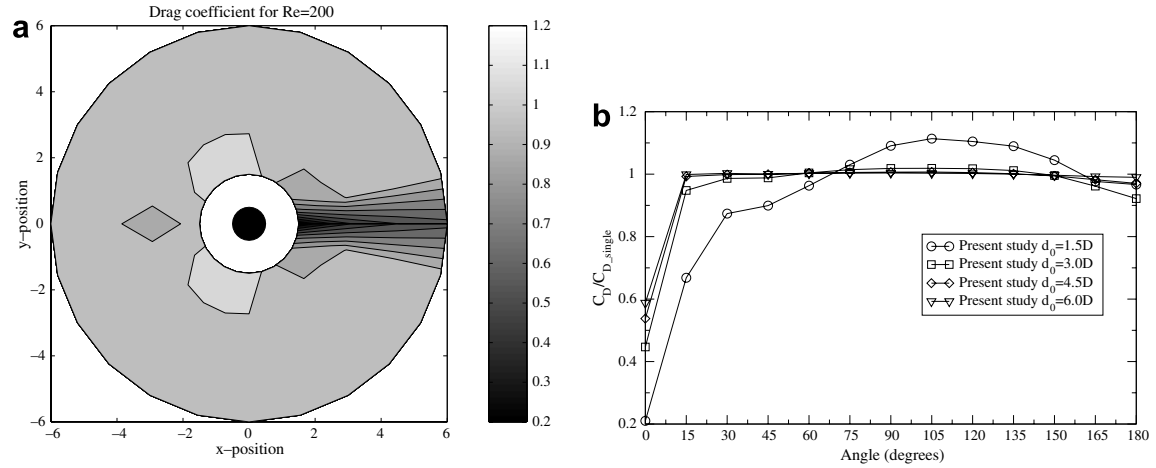

Fig. 16. Normalized drag coefficient at $Re = 200$ with a contour plot (a) and as a function of an angle α (b). The black circle represent the reference particle. Data from VOS computations.

been evaluated. VOS used 2.7 s per iteration, whereas the time for LBM(I) and LBM(II) are 2.0 s and 11.0 s, respectively. Comparing VOS and LBM(I) displayed good resemblance, leading to the conclusion that there is no obvious choice of method from the computational point of view.

4.2. Twin particles

Contour plots of drag and lift coefficients for the secondary particle as well as variation of drag and lift as a secondary particle is placed at different locations relative a reference particle starting at a position downstream

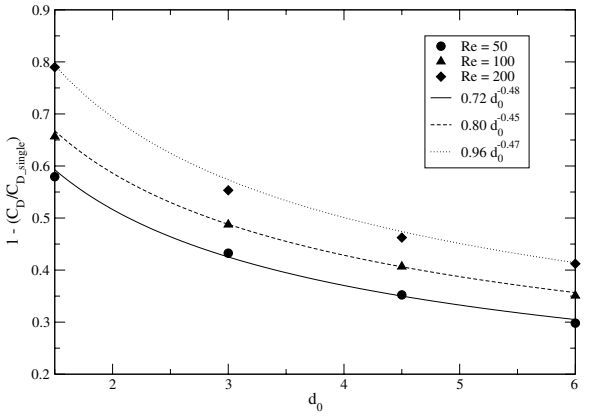

Fig. 17. The change in drag coefficient as a function of the separation distance d_0 for $Re = 50$, 100 and 200 for particles placed in tandem formation.

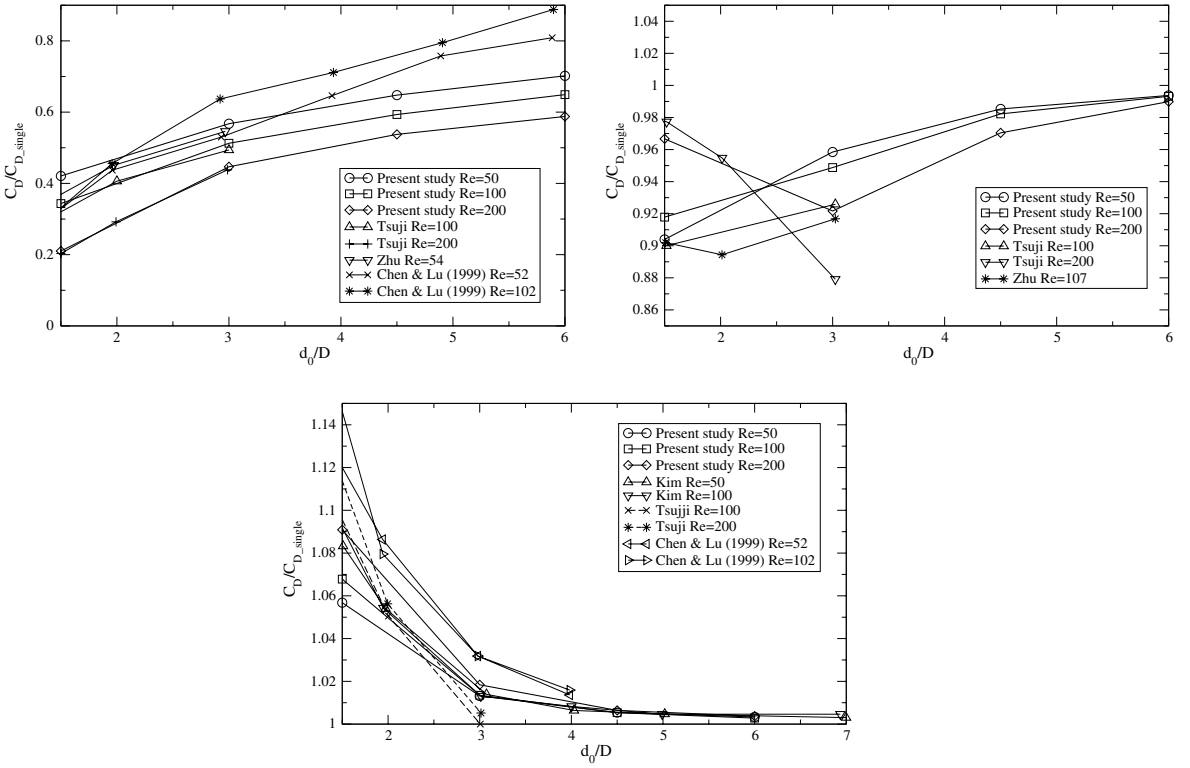

Fig. 18. Normalized drag coefficient for the secondary particle as a function of distance for $\alpha = 0°$ (upper left), $\alpha = 180°$ (upper right) and $\alpha = 90°$ (bottom).

of the reference particle are displayed in Figs. 14–16 (drag) and 21–23 (lift) for $Re = 50$, 100 and 200. It should be noted that C_D is normalized by the drag of a single particle for the Reynolds number of interest whereas C_L is left unchanged.

Regarding C_D, a mutual feature for the different Reynolds numbers is that the largest change in drag occurs for the tandem arrangement. Considering Figs. 14–16, the width of the downstream area where the reference particle affects the drag of a secondary particle is narrowed and elongated as the Reynolds number is increased. The three contour plots indicate that as the particles are moved further apart, the reference particle has less impact on the secondary particle. The maximum drag reduction for the secondary particle in a tandem

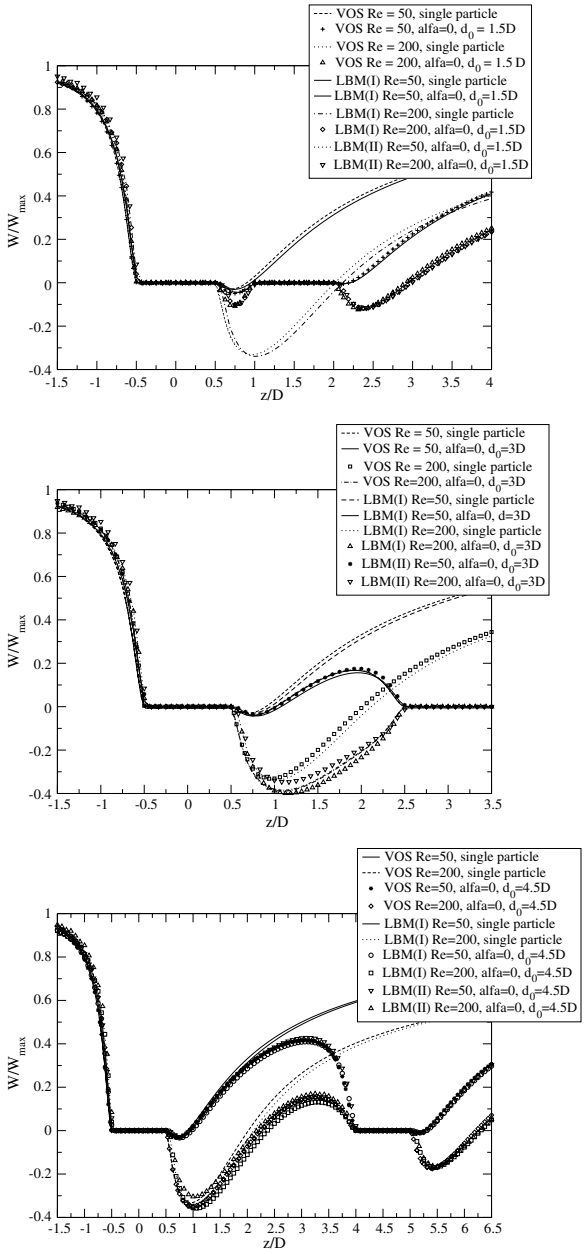

Fig. 19. Velocity profiles at $Re = 50$ and 200 in streamwise direction through the sphere centerline. The dual particles in tandem formation with separation distances of 1.5D (top), 3.0D (middle) and 4.5D (bottom).

formation compared to a single particle is as high as 60%, 70% and 80% for $Re = 50$, 100 and 200, respectively. Furthermore, for particles placed in tandem, the change in drag is found to closely correspond to $d_0^{-\varepsilon}$, where the constant ε is within the interval 0.45–0.48 depending on the Reynolds number (Fig. 17).

Since the results obtained using VOS, LBM(I) and LBM(II) are close to identical, only results from VOS simulations are show here. As observed in Figs. 14–16, the present data show good agreement with numerical simulations presented by Olsson and Fuchs (1998). For Reynolds numbers of 50 and 100, the experimental results of Chen and Wu (2000) show a similar trend of drag compared to present data.

At separation distances of $1.5D$ and angles within the interval 75–135° for $Re = 50$, the secondary particle is subjected to a drag greater than that of a single particle. The same feature is also depict for higher Reynold numbers, with drag greater than that of an isolated particle occuring at $\alpha = 75°$, but up to an angle of 165° for $Re = 200$. In the experimental study of Chen and Wu (2000), maximum drag was estimated to 1.2 times the

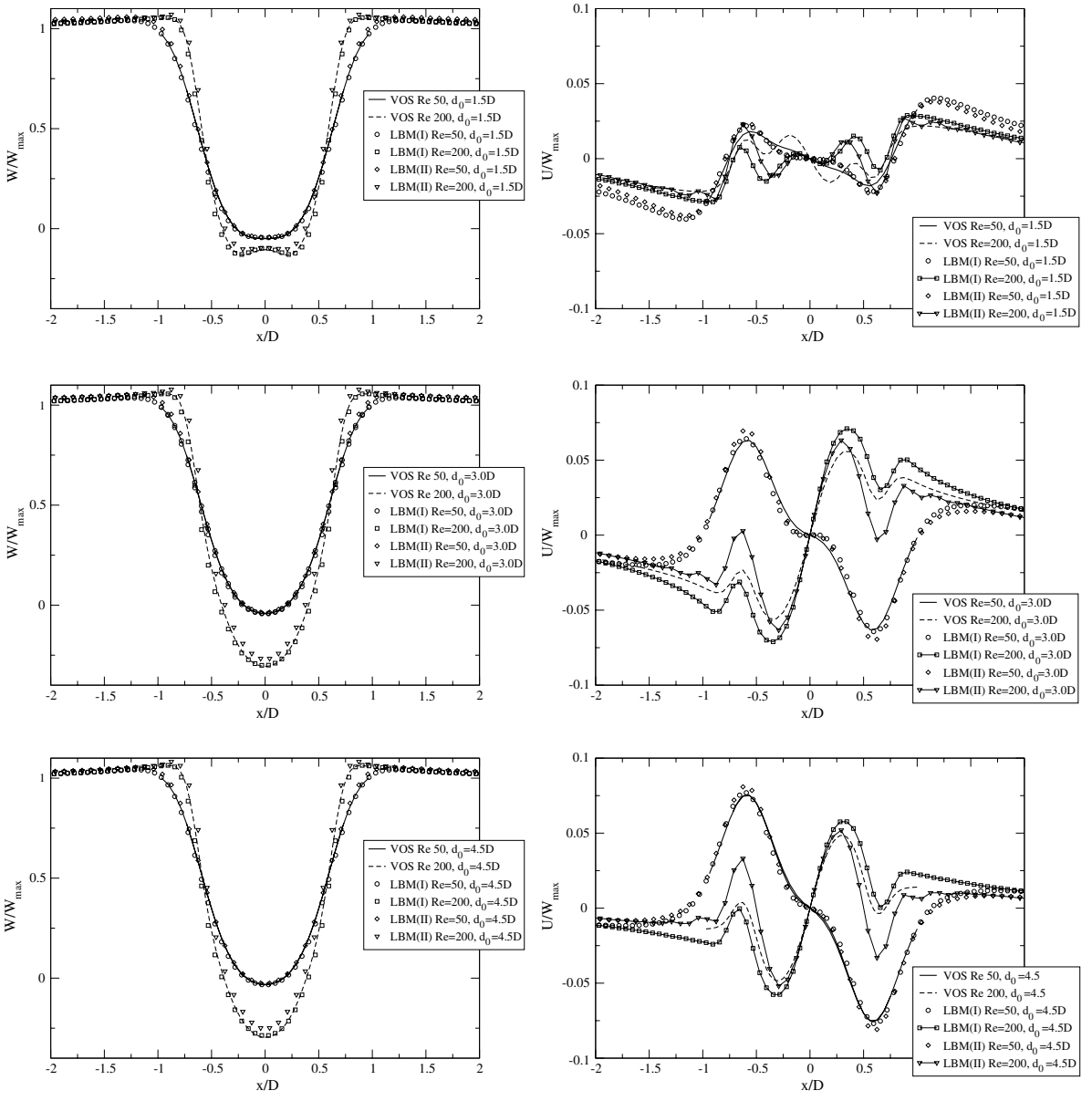

Fig. 20. Velocity profiles $0.75D$ behind the reference particle for $\alpha = 0°$.

drag of an isolated particle and occured at an angle of 120° for $Re = 100$, whereas present results predicts the maximum value of approximately 1.1 at angle of 105–120°.

Fig. 18(upper left) depicts the drag of a secondary particle for 0° and the results show good agreement with present data and results from Tsuji et al. (2003). Considering how the drag reduction varies with sphere distance the present results show the same trend as the experimental data by Chen and Lu (1999) although the experiments show a somewhat lower reduction. However, concerning the Reynolds number dependency, the data by Chen and Lu (1999) shows an opposite trend as compared to present results and results by Tsuji et al. (2003). In order to explain this, further investigation would be needed. Considering the secondary particle for $\alpha = 180°$, the drag coefficient shows different trends depending on Reynolds number (Fig. 18 (upper right)). Reynolds numbers of 50 and 100 show similar features, but as the Reynolds number is increased to 200, the drag is closer to that of a single particle compared to the two lower Reynolds number cases for $d_0 = 1.5D$. However, increasing the separation distance for the particle placed at $\alpha = 180°$ to $3.0D$, leads to a decrease in drag for $Re = 200$, whereas C_D for the two lower Reynolds number increases. An explanation is found in the development of the wake of the reference particle. For single particle flow, with a Reynolds number of 100, previous simulations and experiments have predicted the wake to have a length of 0.84 –

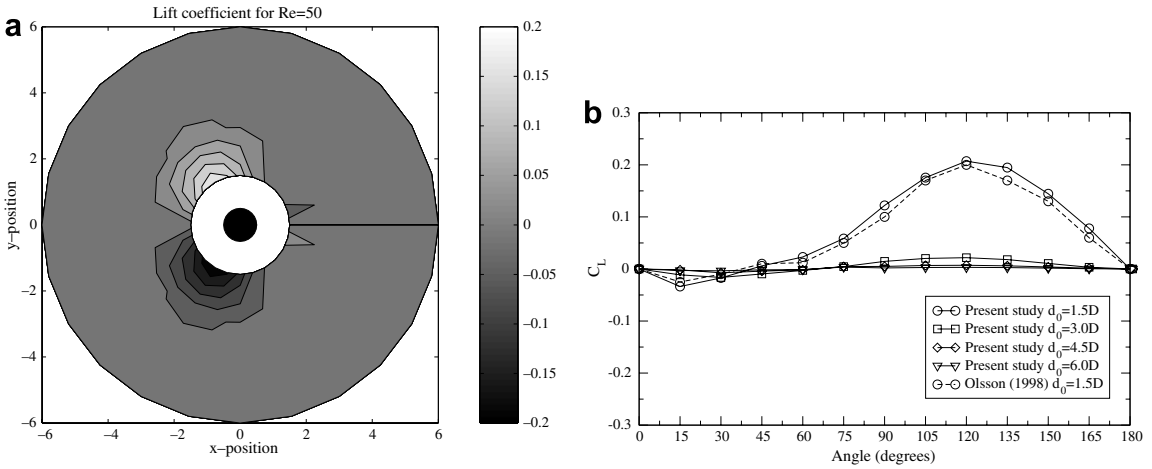

Fig. 21. Lift coefficient at $Re = 50$ with a contour plot (a) and as a function of an angle α (b). The black circle represent the reference particle. Data from VOS computations.

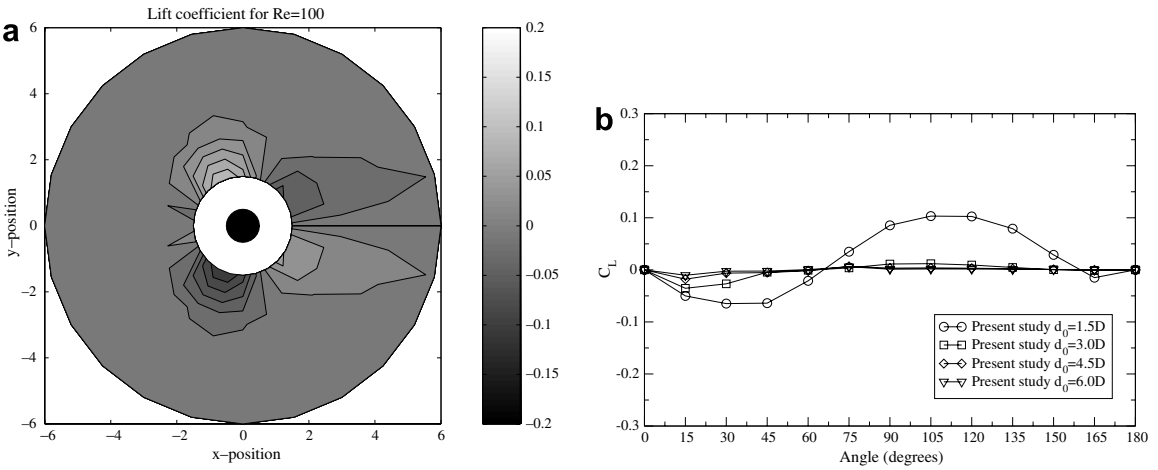

Fig. 22. Lift coefficient at $Re = 100$ with a contour plot (a) and as a function of an angle α (b). The black circle represent the reference particle. Data from VOS computations.

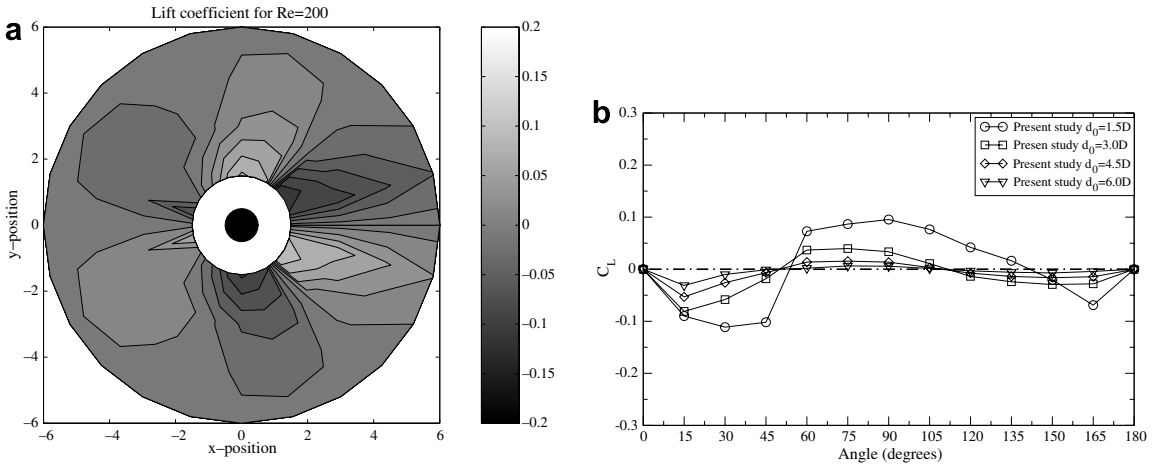

Fig. 23. Lift coefficient at $Re = 200$ with a contour plot (left) and as a function of an angle α (right). The black circle represent the reference particle. Data from VOS computations.

$0.93D$ (Shirayama, 1992; Pruppacher et al., 1970). Increasing the Reynolds number will lead to an increase in wake length. Fig. 13 depicts how the secondary particle is interfering with the wake of the reference particle at a separation distance of $3.0D$ and $\alpha = 15°$. As explained by Tsuji et al. (2003), the separated flow from the reference particle forms ring-like vorticies in the wake region between the two particles, vortices which appears to be isolated from the main flow. Considering Fig. 19, showing profiles of the streamwise velocity component in the center plane, it is evident how the secondary particle interferes with the wake of the reference particle, especially for $Re = 200$. For Reynolds number 50, the wake has time to fully develop even at small separation distances. Also, the velocity field appears to be strongly effected by the separation distance for the higher Reynolds numbers. As the distance is increased, the velocity profile in the wake region almost coincides with the velocity profile of a single particle (the dashed line). Fig. 20 shows the streamwise and the transversal velocity component taken $0.75D$ behind the reference particle in a tandem formation for $Re = 50$ and 200 and $D_0 = 1.5$, 3.0 and $4.5D$. Again, the differences between the solvers are marginal.

As mentioned in the introduction, a common arrangement when studying interactive particles is the side-by-side formation. At small separation distances, the particles experience higher drag. As the distance between the particles approaches $d_0 = 6D$, the drag levels of to that of an isolated particle (Fig. 18 (bottom)).

Compared to drag, the situation for the lift force, the force acting perpendicular to the undisturbed flow, is somewhat different, Figs. 21–23. For Reynolds numbers of 50 and 100, the largest lift is found for a secondary particle placed in the zone slightly upstream the reference particle at a separation distance of $d_0 = 1.5D$, where the particles repel each other. Placed at $d_0 = 1.5D$, the velocity in the gap between the particles is low, indicating a high-pressure region. Due to the high pressure, the fluid will force the particle towards the lower pressure region. However, repulsion forces are not as strong for $Re = 100$ as for $Re = 50$. With increasing Reynolds number (both 100 and 200), attraction forces, due to the low pressure region between the particles, are found in the area downstream the reference particle. At a Reynolds number of 50, this occurs for $d_0 = 1.5D$. However, for $Re = 200$, this feature is also observed at larger separation distances. The results in Figs. 21–23, can provide an general idea of the particle dynamics. A common feature for $Re = 100$ and $Re = 200$, not visible for $Re = 50$, is that a particle placed at an angle around 60° for $d_0 = 1.5D$, is not subjected to any lift force. However, the particle could still experience a repulsive force due to difference in drag.

5. Conclusions

The interaction among dual particles for various particle arrangements and Reynolds numbers of 50, 100 and 200 has been investigated using Volume of Solid (VOS) and Lattice Boltzmann Method (LBM). No significant difference in terms of accuracy and computational efficiency of the VOS and LBM approaches have

been found. Both VOS and LBM show similar behaviour when comparing computations of velocity components as well as drag and lift forces resulting from the different solvers. Both particle Reynolds number and the relative position of two spherical particles are found to influence the drag and lift force the particles are subjected to. The strongest effect on drag force when including a second particle in the flow compared to a single particle case appears for tandem arrangements. The drag reduction for a tandem arrangement is as high as 60%, 70% and 80% for $Re = 50$, 100 and 200, respectively. When placed with a small separation distance in a side-by-side arrangement, the secondary particle is found to experience a slightly higher drag compared to a single particle. Due to high and low pressure regions in the areas between the particles, the particles experience repulsion and attraction forces, respectively. The largest lift force is found in a formation where the secondary particle is placed slightly upstream the reference particle at a small separation distance where repulsion forces appear. In the low pressure region occurring in the area downstream of the reference particle, particles experience attraction forces for Reynolds numbers of 100 and 200. The results emphasize the need for introducing new models for accounting for the lift and drag coefficients within the Lagrangian Particle Transport model framework. Such models can be based on the results shown here.

Acknowledgements

The work herein has been partially (L. Prahl) supported by the Swedish Research Council (VR) and (A. Hölzer) by the EU Marie Curie fellowship program.

References

Aidun, C.K., Lu, Y., Ding, E.-J., 1998. Direct analysis of particulate suspensions with inertia using the discrete Boltzmann equation. J. Fluid Mech. 373, 287–311.

Bhatnagar, P.L., Gross, E.P., Krook, M., 1954. A model for collision processes in gases. Small amplitude processes in charged and neutral one-component system. Phys. Rev. 94, 511–525.

Bouzidi, M., Firdaouss, M., Lallemand, P., 2001. Momentum transfer of a lattice-Boltzmann fluid with boundaries. Phys. Fluids 13, 3452–3459.

Brydon, A.D., Thompson, M.C., 2001. Flow interaction between two spheres at moderate Reynolds numbers. In: 14th Australasian Fluid Mech. Conf., Adelaide, Australia, 10–14 December 2001.

Chen, R.C., Lu, Y.N., 1999. The flow characteristics of an interactive particle at low Reynolds numbers. Int. J. Multiphase Flow 25, 1645–1655.

Chen, R.C., Wu, J.L., 2000. The flow characteristics between two interactive spheres. Chem. Eng. Sci. 55, 1143–1158.

Dupuis, A., 2002. From a lattice Boltzmann model to a parallel and reusable implementation of a virtual river, PhD Thesis, University of Geneva, Geneva, Switzerland.

Eveson, G.F., Hall, E.W., Ward, S.G., 1959. Interaction between two equal-sized equal-settling spheres moving through a viscous liquid. Br. J. Appl. Phys. 10, 43–47.

Faxen, H., 1925. Gegenseitige Einwirkung zweier Kugeln, die in einer zähen Flüssigkeit fallen. Ark Mat., Astron Fys. 19A (13), 1–8.

Faxen, H., 1927. Die Geschwindigkeit zweier Kugeln, die unter Einwirkung der Schwere in einer zähen Flüssigkeit fallen. Z. Angew. Math. Mech. 7, 79–80.

Folkersma, R., Stein, H.N., van de Vosse, F.N., 2000. Hydrodynamic interactions between two identical spheres held fixed side by side against a uniform stream directed perpendicular to the line connecting the spheres' centers. Int. J. Multiphase Flow 26, 877–887.

Fornberg, B., 1988. Steady viscous flow past a sphere at high Reynolds numbers. J. Fluid Mech. 190, 471–489.

Gullbrand, J., Bai, X.-S., Fuchs, L., 2001. High-order Cartesian grid method for calculation of incompressible turbulent flow. Int. J. Numer. Methods Fluids 36, 687–709.

Happel, J., Brenner, H., 1965. Low Reynolds Number Hydrodynamics. Marinus Nijhoff Publishers, The Hague.

Happel, J., Pfeffer, R., 1960. The motion of two spheres following each other in a viscous fluid. AIChE J. 6, 129–133.

Johnson, T.A., Patel, V.C., 1999. Flow past a sphere up to a Reynolds number of 300. J. Fluid Mech. 378, 19–70.

Kim, I., Pearlstein, A., 1990. Stability of the flow past a sphere. J. Fluid Mech. 211, 73–93.

Kim, I., Elghobashi, S., Sirignano, W.A., 1993. Three-dimensional flow over two spheres placed side by side. J. Fluid Mech. 246, 465–488.

Ladd, A.J.C., 1994. Numerical simulations of particulate suspensions via a discretized Boltzmann equation. J. Fluid Mech. 271, 285–309.

Lee, S., 2000. A numerical study of the unsteady wake behind a sphere in a uniform flow at moderate Reynolds numbers. Comput. Fluids 29, 639–667.

Liang, S.-C., Hong, T., Fan, L.-S., 1996. Effects of particle arrangements on the drag force of a particle in the intermediate flow regime. Int. J. Multiphase Flow 22 (2), 285–306.

Lörstad, D., Fuchs, L., 2001. A volume of fluid (VOF) method for handling solid objects using fixed Cartesian grids. In: Sarler, B., Brebbia, C.A. (Eds.), Moving Boundaries VI – Computational Modelling of Free and Moving Boundary Problems. Wessex Institute of Technology, WIT Press, UK, pp. 143–152.

Nakabayshi, K., Aoi, T., 1989. Comparison of the analytical solutions with numerical solutions for viscous flows past a sphere. Nagare 8, 48–55 (in Japanese).

Natarajan, R., Acrivos, A., 1993. The instability of the steady flow past spheres and disks. J. Fluid Mech. 254, 323–344.

Olsson, P.J., Fuchs, L., 1998. The interaction of spherical particles in a fluid flow governed by Navier–Stokes Equations. In: Papailiou, K.D., et al. (Eds.), In: Proceedings of the Fourth ECCOMAS Conference on Computational Fluid Dynamics'98, 1. John Wiley & Sons, pp. 180–185.

Pruppacher, H.R., Le Clair, B.P., Hamielec, A.E., 1970. Some relations between drag and flow pattern of viscous flow past a sphere and a cylinder at low and intermediate Reynolds numbers. J. Fluid Mech. 44, 781–790.

Qian, Y.H., d'Humieres, D., Lallemand, P., 1992. Lattice BGK models for Navier–Stokes equation. Europhys. Lett. 17, 479–484.

Rowe, P.N., Henwood, G.A., 1961. Drag forces in a hydraulic model of a fluidised bed – part 1. Trans. Inst. Chem. Eng. 39, 43–54.

Schlichting, H., 1955. Boundary-Layer Theory. McGraw-Hill, New York.

Shirayama, S., 1992. Flow past a sphere: topological transitions of the vorticity field. AIAA J. 30 (2), 349–358.

Smoluchowski, M., 1911. Über die Wechselwirkung von Kugeln, die sich in einer zähen Flüssigkeit bewegen. Bull. Int. Acad. Sci. Cracovie Series A 1, 28–39.

Stimson, M., Jeffery, G.B., 1926. The motion of two spheres in a viscous fluid. Proc. Roy. Soc. London A 111, 110–116.

Taneda, S., 1956. Experimental investigation of the wake behind a sphere at low Reynolds number. J. Phys. Soc. Jpn. 11, 302–307.

Tomboulides, A.G., Orszag, S.A., 2000. Numerical investigation of transitional and weak turbulent flow past a sphere. J. Fluid Mech. 416, 45–73.

Tsuji, T., Narutomi, R., Yokomine, T., Ebara, S., Shimizu, A., 2003. Unsteady three-dimensional simulation of interactions between flow and two particles. Int. J. Multiphase Flow 29, 1431–1450.

Wieselberger, C., Betz, A., Prandtl, L., 1923. Ergebnisse der Aerodynamischen Versuchsanstalt zu Göttingen. Technical Report, Universität Göttingen.

Zhu, C., Liang, S.C., Fan, L.-S., 1994. Particle wake effects on the drag force of an interacting particle. Int. J. Multiphase Flow 20, 117–129.